Nuclear Inst. and Methods in Physics Research, A 895 (2018) 10–18

Contents lists available at ScienceDirect

Nuclear Inst. and Methods in Physics Research, A

journal homepage: www.elsevier.com/locate/nima

Compensation of orbit distortion due to quadrupole motion using feed-forward control at KEK ATF

D.R. Bett [a,*], C. Charrondière [a], M. Patecki [a], J. Pfingstner [a], D. Schulte [a], R. Tomás [a], A. Jeremie [b], K. Kubo [c], S. Kuroda [c], T. Naito [c], T. Okugi [c], T. Tauchi [c], N. Terunuma [c], P.N. Burrows [d], G.B. Christian [d], C. Perry [d]

[a] European Organization for Nuclear Research (CERN), Geneva 23, CH-1211, Switzerland
[b] Laboratoire d'Annecy-le-Vieux de Physique des Particules (LAPP), Université Savoie Mont Blanc, CNRS/IN2P3, F-74941 Annecy, France
[c] KEK and SOKENDAI, 1-1 Oho, Tsukuba, Ibaraki 305-0801, Japan
[d] University of Oxford, Keble Road, OX1 3RH, UK

ARTICLE INFO

Keywords:
Linear collider
Ground motion
Beam stability

ABSTRACT

The high luminosity requirement for a future linear collider sets a demanding limit on the beam quality at the Interaction Point (IP). One potential source of luminosity loss is the motion of the ground itself. The resulting misalignments of the quadrupole magnets cause distortions to the beam orbit and hence an increase in the beam emittance. This paper describes a technique for compensating this orbit distortion by using seismometers to monitor the misalignment of the quadrupole magnets in real-time.

The first demonstration of the technique was achieved at the Accelerator Test Facility (ATF) at KEK in Japan. The feed-forward system consisted of a seismometer-based quadrupole motion monitoring system, an FPGA-based feed-forward processor and a stripline kicker plus associated electronics. Through the application of a kick calculated from the position of a single quadruple, the system was able to remove about 80% of the component of the beam jitter that was correlated to the motion of the quadrupole. As a significant fraction of the orbit jitter in the ATF final focus is due to sources other than quadrupole misalignment, this amounted to an approximately 15% reduction in the absolute beam jitter.

1. Introduction

The dynamic misalignment of the beamline components of a future linear collider results in beam imperfections such as increased emittance [1] and position offsets at the Interaction Point (IP) [2]. Several mitigation schemes exist for the purpose of compensating for the motion of such components.

The technique of beam orbit feedback [3] uses at least one beam position monitor (BPM) to track the position of the beam and one corrector magnet to restore it to its nominal orbit. Such systems are limited by the frequency at which the BPM data is generated. For a single-pass machine this is the machine repetition rate, which corresponds to 5 Hz for the International Linear Collider (ILC) [4] and 50 Hz for the Compact Linear Collider (CLIC) [5]. Other techniques include faster intra-bunch train feedbacks [6] as well as stabilization of the quadrupole magnets themselves, both active [7–9] and passive [10].

The novel technique of compensation of orbit distortion due to quadrupole motion using feed-forward control [11] is similar in concept to beam orbit feedback but the measured displacement of a quadrupole is used to determine the deflection to provide to the beam, instead of the position of the beam itself (Fig. 1). The primary benefit of such a system is that it can correct frequencies higher than the beam repetition rate.

A theoretical framework for such a system is presented in detail in [11]. This paper describes the quadrupole motion monitoring system deployed at the KEK Accelerator Test Facility (ATF), a test accelerator whose primary goal is the generation of very low emittance electron beams, and then summarizes the results obtained with that system and what they said about the relationship between the position of the quadrupoles and the beam orbit in the final focus region of ATF. Section 3 describes the additional hardware that was used to add the feed-forward correction functionality to the system and Section 4 presents the results obtained when the feed-forward system was operated in June 2017.

* Corresponding author.
E-mail address: douglas.bett@physics.ox.ac.uk (D.R. Bett).

https://doi.org/10.1016/j.nima.2018.03.037
Received 29 November 2017; Received in revised form 5 March 2018; Accepted 10 March 2018
Available online 26 March 2018

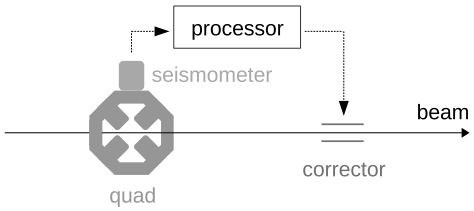

Fig. 1. Schematic illustrating the principle of compensation of orbit distortion due to quadrupole motion using feed-forward control.

2. Measuring the effect of quadrupole motion on beam orbit

The extent to which the beam orbit depends on the motion of the quadrupoles determines the amount of stabilization that could be achieved using a quadrupole motion feed-forward system. This section describes how the correlation between the quadrupole positions and the beam orbit was determined at ATF [12]. As the beam required for a future linear collider is so much smaller in the vertical axis than in the horizontal, small vertical displacements of the quadrupoles will have a much greater impact on the luminosity compared to horizontal displacements. The analysis presented here thus concerns only the vertical positions of the quadrupoles and the beam.

2.1. Hardware

The motion of the quadrupoles is determined using a set of 14 Güralp 6T seismometers [13] installed at ATF by the Laboratoire d'Annecy-le-Vieux de Physique des Particules (LAPP). The nominal locations of the seismometers at ATF are indicated in Fig. 2 [14]. The issue of their exact placement is the subject of Section 2.3.1 and the conclusion is that they are optimally located on top of the quadrupole magnets as depicted in Fig. 3. Each seismometer produces an output proportional to their velocity in both directions perpendicular to the direction of beam travel.

The seismometer outputs are digitized and logged using a National Instruments PXI system provided by CERN. This system consists of a PXI-1042 chassis with a PXI-8108 controller and two PXI-6289 multi-function DAQ modules to provide the necessary analogue-to-digital converters (ADCs). The measured voltages are logged to file and the position is determined by first converting the measured voltage to a velocity using the sensor calibration constant and then integrating the result.

The ATF BPMs are mostly of the cavity type and have a resolution better than 1 μm [15]. The raw BPM signals are processed in real time and the results are published to an EPICS [16] database at the machine repetition rate of 3.12 Hz. This database also contains a measurement of the beam intensity which is logged on a pulse-by-pulse basis alongside the beam position data [17].

2.2. Data acquisition

As the seismometers can measure signals up to 100 Hz in frequency, the minimum sampling rate required for the seismometer outputs is the Nyquist rate of 200 Hz. This means that there will be many more samples in the seismometer data set (one every 5 ms) compared to the BPM data set (one every ~320 ms). For correlation studies, the beam position should be compared with the position of the seismometers at the moment of beam arrival. In order to identify the relevant samples of the seismometer data set, the PXI system was used to record an additional signal referred to as the "synchronization signal".

The generation of this synchronization signal is illustrated in Fig. 4. The signal from a beam charge monitor is first put through a discriminator module which performs a threshold check. The output of the discriminator is then input to a coincidence module, along with a copy of the extraction kicker trigger signal. The extraction kicker trigger consists of a 0.5 μs pulse that precedes the arrival of the beam at the extraction kicker by 10 μs. The overlap of these two signals is used as the trigger for a gate/delay generator module. The output of this module is the synchronization signal, a stretched version of the kicker trigger pulse that is only present if the bunch charge exceeds the threshold set in the discriminator.

The width of a synchronization signal pulse is approximately 2 ms and so the ADCs of the PXI system are clocked at 1024 Hz to ensure that the pulses are detected reliably. As the rising edge of each pulse approximately coincides with the extraction of the beam from the damping ring, the rising edges in the synchronization signal data set identify the subset of samples from the seismometer position data set that corresponded to when the beam was present. This subset of samples will ultimately be compared with the beam position data in the analysis.

In addition to indicating which samples should survive the down-sampling of the seismometer data set to 3.12 Hz, the synchronization signal also carries valuable information about the beam on/off status on a pulse-by-pulse basis. This is useful as the beam intensity is also stored along with the BPM data. By starting the data acquisition with the beam turned off and turning it on shortly afterwards, and then turning the beam off again just before the acquisition is complete, a pair of reference points are created in both data sets that can be used to verify that the two are synchronized.

2.3. Results

The analysis is performed using the numerical computation software Octave [18]. A single data run includes the seismometer position data as a function of time (which represents the position offsets of the quadrupoles) and the beam position data y_m. Both are measured over a period of approximately 15 min. The seismometer data is gathered at a frequency of 1024 Hz and the synchronization signal is used to down-sample it to 3.12 Hz to match the BPM data. As an offset quadrupole imparts a kick to the beam proportional to the magnitude of the offset, the analysis fits the vector y_r which is the reconstruction of the beam position as a linear combination of the quadrupole offsets. An alternative and conceptually equivalent approach would be to weight each quadrupole by the R_{34} element of the quadrupole-BPM transfer matrix; however, to account for any discrepancy between model and reality, the fitted value was used instead. Note that the vibrations of the BPM itself are neglected so that the measured and reconstructed beam position can be considered to share a common set of coordinates. The potential of the feed-forward system can then be judged by the Pearson correlation coefficient r calculated between this reconstruction of the beam position and the actual measurement:

$$r = \frac{\mathrm{cov}(y_r, y_m)}{\sigma_{y_r}\sigma_{y_m}} \tag{1}$$

where $\mathrm{cov}(y_r, y_m)$ is the covariance of the two variables and σ_{y_r} and σ_{y_m} are the standard deviations of the reconstructed beam position and the measured beam position respectively. r^2 then gives the proportion of the variance in the beam position that is predictable from the quadrupole offsets. Assuming an ideal system that is capable of completely removing the component of the beam position that is correlated with the positions of the quadrupoles, the jitter reduction factor that would be achieved is:

$$\frac{\sigma_f}{\sigma_i} = \sqrt{1 - r^2} \tag{2}$$

where σ_f is the jitter of the corrected beam and σ_i is the jitter of the uncorrected beam.

Previous studies of the seismometer performance indicated that the coherence between the measured position for a pair of adjacent seismometers is consistent with zero below a cutoff frequency of about 0.2 Hz [19]. This finding, along with the 100 Hz maximum frequency specified by the manufacturer, motivated the application of a band-pass filter with limits of 0.2 and 100 Hz to the seismometer data before attempting to correlate it with the beam position data.

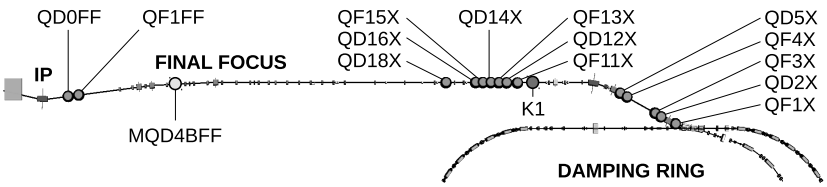

Fig. 2. Schematic of the ATF. The beam circulates in an anticlockwise direction around the damping ring until extraction, after which it travels down the Final Focus section to the notional IP (from right to left on the page). Three types of beamline components are labelled: quadrupole magnets equipped with seismometers (QF1X etc.), the stripline kicker K1 and the cavity BPM MQD4BFF. The diagram is to scale and the distance from extraction to the IP is approximately 90 m.

Fig. 3. Photograph of the seismometer mounted on quadrupole QF4X.

A second-order Butterworth filter [20] is used. Several important conclusions could be drawn from the results of the correlation studies: first, that the exact placement of the seismometers had a large effect on the correlations that were observed; second, that motion of the quadrupole QD2X was the dominant cause of the observed correlation; and third, that the observed correlations could be improved through the application of an optimized band-pass filter to the seismometer data.

2.3.1. Seismometer placement

It was originally supposed that mounting the seismometers on the tables supporting the quadrupoles would be just as good as placing the seismometers directly on the quadrupoles themselves. Fig. 5 shows the correlation between the reconstructed vertical beam position and the actual measurement from each cavity BPM in the final focus for four different data runs taken in May 2015. For the 11:13 and 11:40 data runs the seismometers were placed on the tables close to the quadrupoles. They were then moved on top of the quadrupoles for the 14:15 and 14:30 data runs. In each case the reconstructed beam position is the linear combination of the vertical position of the first five seismometers that best matches the measured vertical position for each BPM. It is clear that placing the seismometers directly on top of the quadrupoles greatly enhances the correlation that can be achieved, increasing it by a factor of 1.75.

It can also be seen that beyond the 50 m mark the correlation is not a function of location in the beamline (with the exception of a few BPMs which are located at image points of the virtual IP). For the

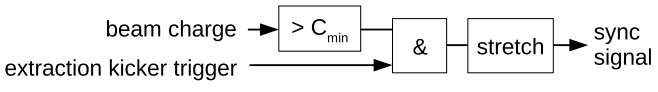

Fig. 4. Schematic of the synchronization signal generation scheme.

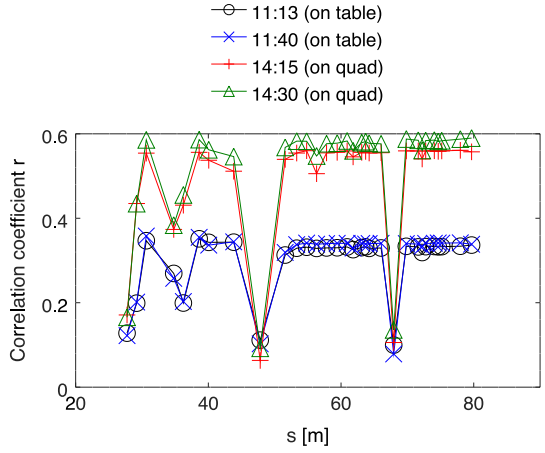

Fig. 5. The correlation coefficient r between the position of the beam and the best fit from a linear combination of the position of the seismometers as a function of the distance of the BPM from the extraction kicker.

nominal optics, the majority of the BPMs in the final focus are at the same betatron phase and as a result the BPM–BPM correlation is close to 1. For the purposes of demonstrating the feed-forward concept it was decided to work initially with a single BPM to keep the system as simple as possible. The BPM chosen was MSD4FF ($s = 74.65$ m) which is located in the region of highest jitter in order to maximize the signal-to-noise ratio.

2.3.2. Dominance of QD2X motion

The change in beam position Δy_b due to the displacement of a single quadrupole by an amount Δy_q is given by:

$$\Delta y_b = R_{34} K_1 L \Delta y_q \tag{3}$$

where R_{34} is the transfer matrix element that describes how the beam position at the BPM depends on the angle of the beam at the quadrupole, $K_1 = \frac{1}{B\rho}\left(\frac{\partial B_y}{\partial x}\right)$ is the normal quadrupole coefficient and L is the quadrupole length. Fig. 6 shows the value of this orbit sensitivity coefficient for the optics used in May 2015. It can be seen that displacements of the quadrupoles QD2X and QD5X are expected to have the largest impact on the orbit of the beam downstream with those further downstream not contributing much at all, and indeed this is largely borne out by the results. Previous studies [11] identified that the cooling water pipes in the QD2X region were a significant source of the vibration and although action was taken to reduce their effect it appears that they remain the dominant cause of vibration-induced beam jitter.

Fig. 7 shows the correlation coefficient calculated between the position of the beam and the position of each of the first twelve seismometers for the 14:30 data run and Fig. 8 shows the correlation that can be achieved when different subsets of seismometers are used to perform the fit. The chart shows that the QD2X seismometer by itself delivers a large correlation of 0.37 and this can be boosted to 0.48 by including data from the adjacent seismometers (QF1X and QF3X) in the fit. A similar increase is observed when the other two seismometers in the upstream part of the extraction line (QF4X and QD5X) are included with the correlation reaching 0.58, but this is the maximum that can be achieved. Even using all twelve of the seismometers upstream of MSD4FF does not significantly improve the correlation beyond this, in line with expectations given the beam optics.

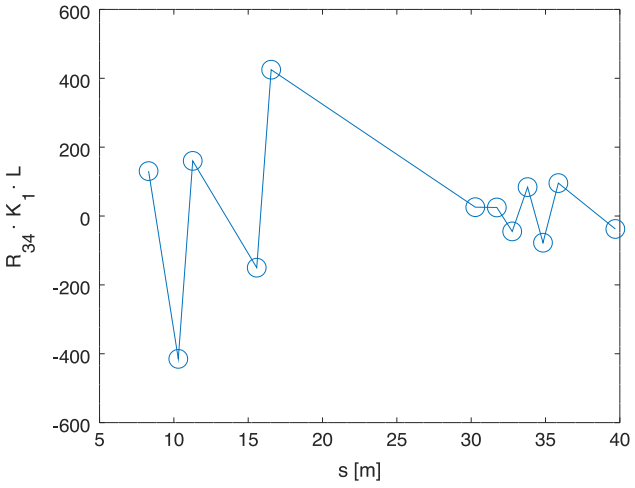

Fig. 6. Sensitivity of the orbit at BPM MSD4FF to displacements of each quadrupole equipped with a seismometer as a function of the distance of the quadrupole from the extraction kicker.

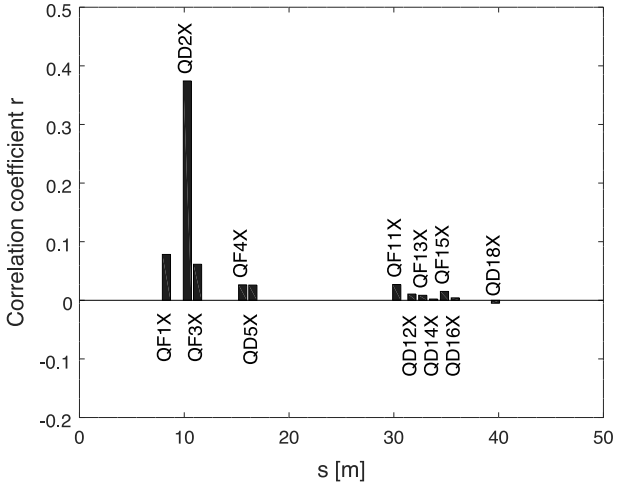

Fig. 7. The correlation coefficient r between the position of the beam at MSD4FF and the position of the individual seismometers for the 14:30 data run as a function of the distance of the seismometer from the extraction kicker.

2.3.3. Filter limits

Fig. 9 shows the power spectral density measured by the seismometer at QD2X for the full 1024 Hz data set. Previous studies carried out with seismometers at ATF identified two pronounced maxima in the QD2X spectrum at 9.94 and 24.25 Hz [11], both of which are clearly visible in Fig. 10, which shows the region from 5 to 30 Hz in more detail. These vibration sources were determined at the time to be due to a pair of cooling water pipes in the QD2X region. However, instead of a single maximum at 24.25 Hz, this newer data shows in that region a series of four narrow peaks at frequencies of 24.14, 24.29, 24.40 and 24.60 Hz. An additional maximum at 11.55 Hz can also be seen.

As described in Section 2.3, a band-pass filter with limits of 0.2 Hz and 100 Hz should be applied to the seismometer data at the very least. Fig. 5 shows that the maximum correlation that can be achieved in this case is 0.58 for the 14:30 data set. An attempt was made to increase the correlation beyond this limit by modifying the passband of the filter that was applied to the seismometer data. Previous studies used a narrowband filter to target specific modes of oscillation of the quadrupole [21]; here the effect of progressively filtering out more of the low frequency range is considered. This is because apparent motion

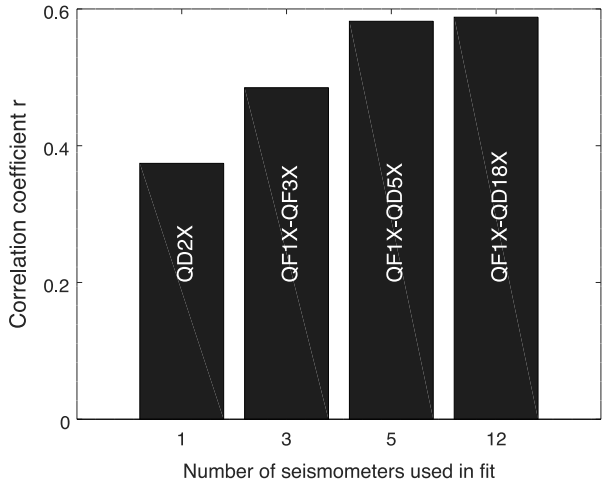

Fig. 8. The correlation coefficient r between the position of the beam at MSD4FF and the best fit from a linear combination of the positions of the seismometers. Each bar represents a different subset of the seismometers as indicated by the label.

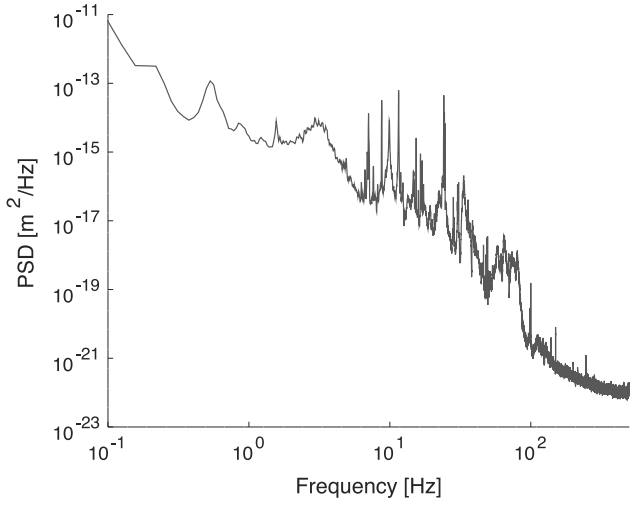

Fig. 9. Power spectral density measured by the seismometer at QD2X.

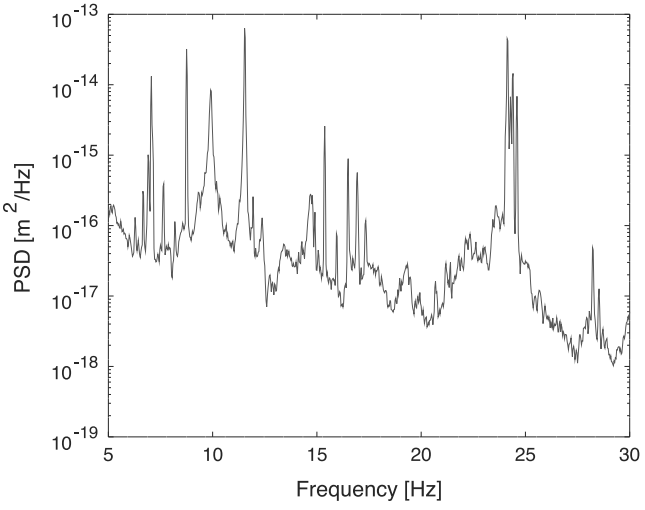

Fig. 10. Power spectral density measured by the seismometer at QD2X in the 5 to 30 Hz range.

Table 1
Frequencies of peaks from the down-sampled seismometer spectrum with matches in the BPM spectrum ($f_{3.12}$) and their unaliased source frequency (f_{1024}).

$f_{3.12}$ [Hz]	f_{1024} [Hz]
0.24	15.38
0.40	24.60
0.60	24.40
0.62	8.75
0.71	24.29
0.82	7.05
0.85	24.14
0.95	11.55

of the seismometer in that region of the spectrum is not reflected in the beam position, presumably as a result of coherent motion of the quadrupole and the BPM at those frequencies.

Fig. 11 compares the power spectral density measured by BPM MSD4FF to that measured by the seismometer at QD2X. Note that the nominal band-pass filter (0.2–100 Hz) has already been applied to the seismometer data and the power spectral density is calculated using Welch's method [22]. Matching peaks at 0.85 and 0.95 Hz are clearly visible in both spectra but there are several features of the seismometer spectrum that are not reflected in the BPM data. Neither the dominant peak at 0.20 Hz nor the broad peak centred at about 0.50 Hz have clear analogues in the BPM spectrum. Removing these signals from the seismometer data may be expected to increase the observed correlation with the BPM data.

It should be noted that the 3.12 Hz sample frequency for both data sets results in aliasing of frequencies higher than 1.56 Hz. The frequencies of the vibration sources driving the beam position are not necessarily the frequencies at which they appear in the spectrum of the down-sampled data. By selective filtering of the 1024 Hz seismometer data set, it was found that the 0.85 Hz and 0.95 Hz peaks in the down-sampled spectrum are due to the vibration sources at 24.14 Hz and 11.55 Hz respectively.

Fig. 12 shows the correlation coefficient r between the position of the beam at MSD4FF and the position of the seismometer on QD2X as a function of the high and low frequency limits of the band-pass filter applied to the seismometer data. The best result of $r = 0.71$ is achieved for a passband of 5 to 100 Hz and including data from the other four of the first five seismometers in the fit increases this slightly to $r = 0.75$. Fig. 13 again compares the power spectral density measured by the BPM at MSD4FF to that measured by the seismometer at QD2X. It is clear that the spectrum of the BPM data is more accurately reproduced when a lower frequency limit of 5 Hz is used for the band-pass filter. This is primarily due to the filtering out of the 0.22 and 0.53 Hz peaks of the seismometer spectrum (Fig. 9). Removing the broad peak in the 2–4 Hz region has the effect of greatly increasing the visibility of a number of peaks that have clear analogues in the BPM data, including one at 0.24 Hz, a second at 0.40 Hz and an overlapping pair with central frequencies of 0.60 and 0.62 Hz. Each frequency in the spectrum of the down-sampled seismometer with a match in the BPM data is listed in Table 1.

2.3.4. Seismometer latency

As described in Section 2.2, the synchronization signal marks the samples of the 1024 Hz data set that will survive the process of down-sampling to 3.12 Hz. These samples are supposed to represent the positions of the seismometers at the point closest in time to when the beam arrived. However, it is possible to perform the analysis using a time-shifted version of the seismometer data set; that is, if the synchronization signal identified that the beam was present for sample X, use sample $X + 1$ instead. As the sample frequency of the data is 1024 Hz, the added delay is about 1 ms per sample.

Fig. 14 shows the correlation coefficient between the position of the beam at MSD4FF and the position of the QD2X seismometer as a

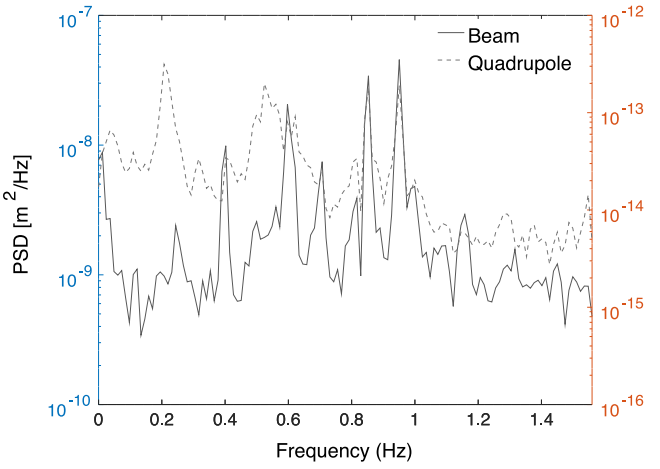

Fig. 11. Power spectral density measured by BPM MSD4FF and by the seismometer at QD2X after down-sampling to 3.12 Hz. A 0.2–100 Hz band-pass filter was applied to the seismometer data prior to down-sampling. The axes on the right corresponds to the quadrupole data.

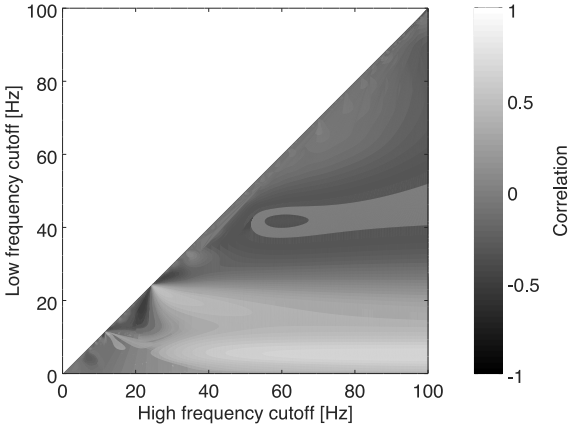

Fig. 12. The correlation coefficient r between the position of the beam at MSD4FF and the down-sampled to 3.12 Hz position of the seismometer at QD2X as a function of the frequency limits of the band-pass filter applied to the seismometer data before down-sampling.

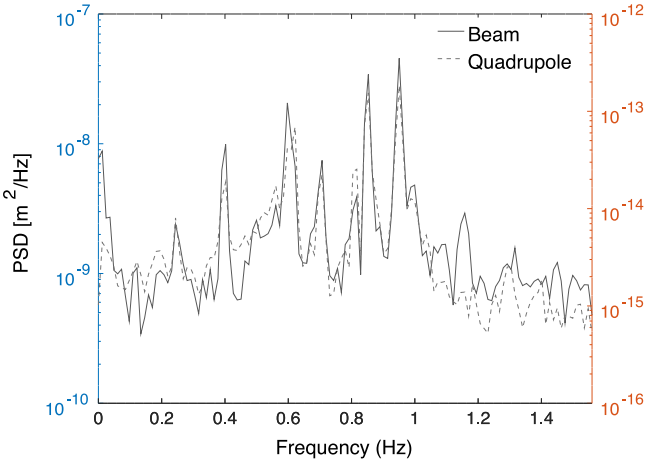

Fig. 13. Power spectral density measured by the BPM at MSD4FF and by the seismometer at QD2X after down-sampling to 3.12 Hz. A 5–100 Hz band-pass filter was applied to the seismometer data prior to down-sampling. The axes on the right corresponds to the quadrupole data.

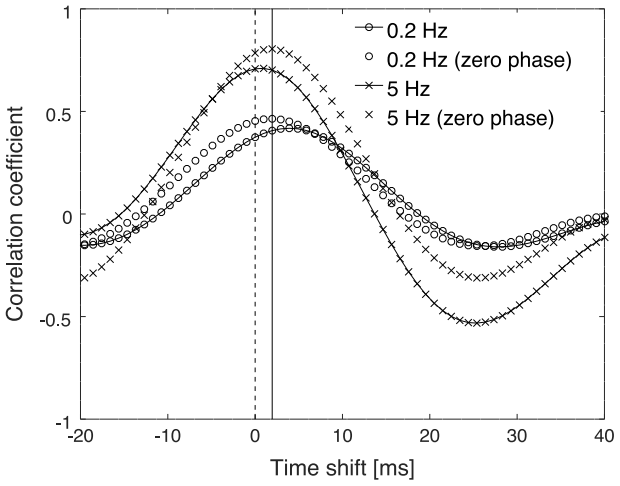

Fig. 14. The correlation coefficient r between the position of the beam at MSD4FF and the fit calculated from the down-sampled to 3.12 Hz position of the seismometer at QD2X as a function of the time shift applied to the seismometer data before down-sampling. A filter with passband X–100 Hz is applied to the seismometer data before down-sampling where X is either 0.2 (circles) or 5 (crosses). The solid vertical black line indicates the time shift that maximized the correlation for the zero phase filters.

function of the time shift applied to the seismometer data. A negative time shift corresponds to performing the fit using the position of the seismometer from a time before the beam arrived. Both minimal filtering (passband 0.2–100 Hz) and optimal filtering (passband 5–100 Hz) cases are considered. Also plotted are the corresponding data for when the filtered data is time-reversed and filtered again in order to produce an output with zero phase distortion relative to the input. Using this procedure the correlation can reach values as high as 0.81 in the case of zero-phase optimal filtering as applying the filter twice results in extra attenuation of the unwanted frequencies. When the same filter is applied once, the corresponding value of the correlation coefficient is 0.71. Such zero-phase filtering cannot be performed in real-time and therefore it is of no relevance to the performance of a feed-forward system. The data reveals that the correlations in the zero-phase case are maximized for a time shift of about 2 ms. This suggests that the synchronization signal does not correctly identify the samples that are closest in time to the arrival of the beam, most likely due to the intrinsic latency of the sensors. In any case, the data for the optimal filtering case shows that this does not significantly affect the correlation that could be achieved in real-time as for the case when a single filter is applied, the correlation for the zero time shift data is very close to the maximum.

3. Implementation of a compensation system for orbit distortions due to quadrupole motion

As depicted in Fig. 1, the feed-forward system at ATF consists of three components. The seismometers that measure the quadrupole displacements were described in Section 2.1 and it has been established that for best results they should be placed directly on top of the quadrupoles. This section deals with the remaining two elements of the feed-forward system: the processor that calculates the compensatory kick and the kicker that applies the calculated correction to the beam.

3.1. Feed-forward processor

The role of the feed-forward processor is filled by a National Instruments CompactRIO (cRIO) system. This FPGA-based unit consists of a cRIO-9064 controller chassis with a cRIO-9205 module for analogue input and a cRIO-9401 module for digital output. The control software is depicted schematically in Fig. 15.

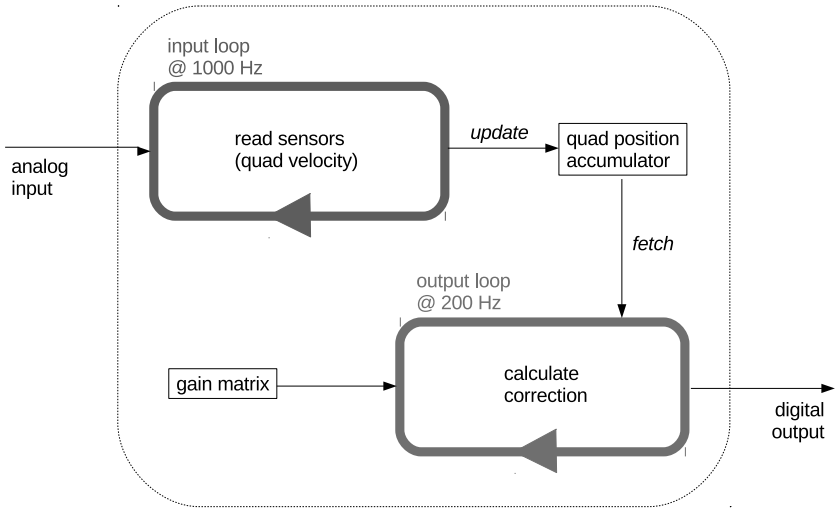

Fig. 15. Schematic of the software running on the feed-forward processor.

The firmware on the FPGA was written in LabVIEW and performs the low-level input and output tasks. The analogue inputs are sampled at a frequency of 1000 Hz and then transferred to the real-time LabVIEW operating system on the cRIO where they are integrated to give the current position of each seismometer. The vector of seismometer positions is then filtered and multiplied by the matrix of gain coefficients to yield the value for the corrective kick. These gain coefficients are determined from a fit of the position at the BPM of interest as a function of the seismometer positions. In the simplest case, the beam position at a single BPM is fitted as a function of the position of a single quadrupole so that there is only one non-zero gain coefficient. The calculated value for the kick is then sent back to the FPGA where it is transmitted as a digital code at a rate of 200 Hz so that the correction is never more than 5 ms out of date. The real-time LabVIEW data acquisition software is also able to store data locally for later transfer to a personal computer for analysis.

3.2. Kicker

The actuator selected for use with the feed-forward system is a simple stripline kicker originating from the SLAC National Accelerator Laboratory [23]. Fig. 16 is a photograph of the kicker in the ATF beamline where it was originally installed as part of the intra-train beam position feedback system developed by the Feedback On Nanosecond Timescales (FONT) group at the University of Oxford [24]. This kicker deflects the beam using the electric field generated when a potential difference is applied across the vertical axis. An ultra-fast, high power amplifier developed by TMD Technologies generates the voltage signals required for this purpose. This amplifier is well beyond the requirements of the feed-forward system but was retained in order to avoid disturbing the existing arrangement of hardware inside the accelerator area.

A custom-made FPGA-based control unit ("FONT5 board" [25]) uses signals from the ATF timing system to produce a trigger for the amplifier that is synchronized with the beam arrival time. When used for its original purpose, the FONT5 board also provides a kicker drive signal based on BPM signals. A more detailed description of the FONT kicker and associated electronics can be found in [23]. Here it is noted that the FONT5 board was already capable of generating constant kicker drive signals for calibration purposes. The only extra functionality required was thus a means of updating this constant value with the current value of the correction calculated by the feed-forward processor. This was performed by modifying the firmware of the FONT5 board to update the amplitude of the kicker drive signal according to the digital code received over the direct connection to the cRIO system.

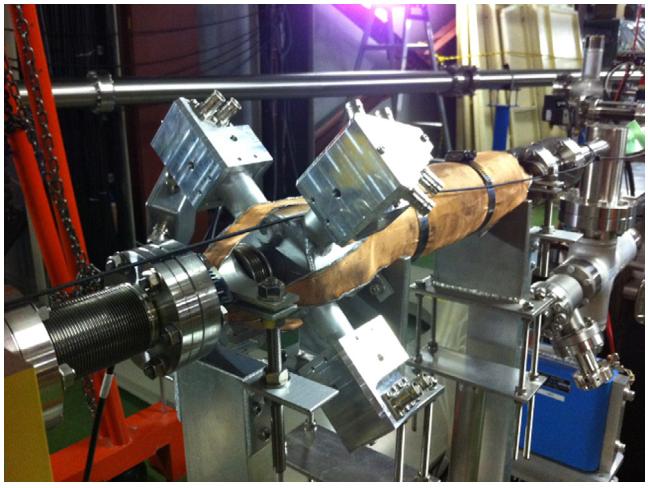

Fig. 16. Photograph of the stripline kicker.

4. Performance of the feed-forward system

The feed-forward system was most recently tested in June 2017. Note that as part of an effort to eliminate wakefield sources in the ATF final focus, several BPMs were removed from the ATF final focus in the period since the studies described in Section 2 were performed. MSD4FF was among those removed and so the adjacent BPM MQD4BFF was used as the BPM of interest for the most recent feed-forward studies.

Each feed-forward data run consisted of a 90 s record of the beam position data (generated at the machine rate of 3.12 Hz) and a slightly longer measurement of the seismometer data (generated at 1000 Hz). The synchronization signal is then used to obtain a set of approximately 250 simultaneous measurements of the position of the beam at MQD4BFF and the position of the quadrupole QD2X.

In order to maximize the performance of the feed-forward system, several control runs were taken in an attempt to accurately assess the correlation between the quadrupole position and the beam position. During this analysis, it was found that reducing the lower frequency cutoff of the band-pass filter applied to the quadrupole position from the 5 Hz optimum estimated from the analysis performed two years prior significantly increased the correlation. Based on this empirical observation of a change in the environment at ATF, the feed-forward algorithm was set to use a 2–100 Hz band-pass filter.

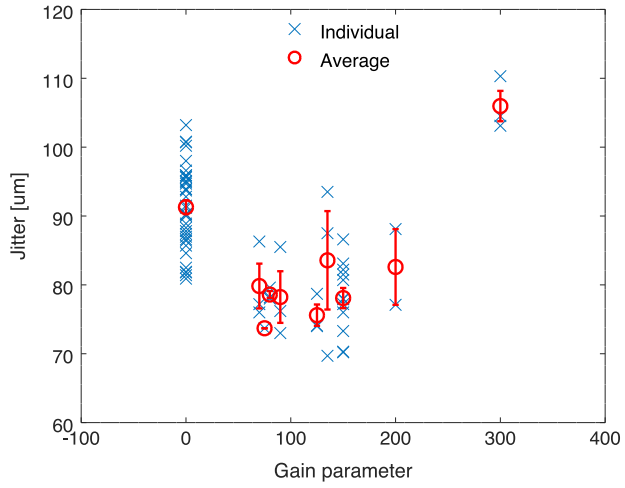

Fig. 17. Beam jitter at MQD4BFF as a function of the gain parameter g. The result for each individual run is shown as a cross and the calculated mean and standard error of the mean for each gain setting is shown as a circle.

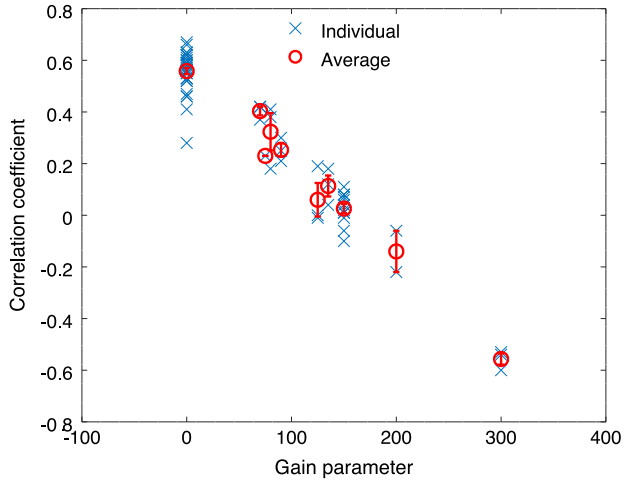

Fig. 18. Correlation between the measured beam position y_m and the reconstructed beam position y_r as a function of the gain parameter g. The result for each individual run is shown as a cross and the calculated mean and standard error of the mean for each gain setting is shown as a circle.

Ultimately many control runs were taken throughout the eight hours allocated for the study and the feed-forward system was operated with a number of different gain settings. Fig. 17 shows the beam jitter measured at MQD4BFF (σ_m) as a function of the feed-forward gain parameter g and Fig. 18 the corresponding value of the Pearson correlation coefficient r between the reconstructed beam position (y_r) and the measurement (y_m). The average beam jitter is smaller for every gain value from 70 to 200 but is increased for a gain as large as 300. The correlation decreases as the gain increases and is approximately zero for the "optimal" gain values of 125, 135 and 150; beyond this, the feed-forward system begins to introduce a negative correlation. The performance of the feed-forward system is summarized in Table 2.

The mean correlation of the zero-gain runs of 0.56 was high compared to previous studies and inserting this value into Eq. (2) suggests that the absolute beam jitter at MQD4BFF could have been reduced by 17% by completely subtracting the component correlated with the position of QD2X. The ratio of the two jitters in Table 2 shows that the feed-forward system in fact achieved a 14% reduction in the beam jitter and, while this represents a modest reduction in absolute terms, an equivalent statement is that the feed-forward system was able to

Table 2
Feed-forward results from the shift on 23 June 2017. σ_b is the average of the vertical jitter of the beam at MQD4BFF, r is the average of the Pearson correlation coefficient between the beam position and the linear reconstruction from the filtered position of quadrupole QD2X and n is the number of runs taken for the given gain setting. Optimal gain refers to the ensemble of runs which had a gain of 125, 135 or 150.

Gain	σ_b [μm]	r	n
Zero	91.3 ± 1.0	0.56 ± 0.01	36
Optimal	78.6 ± 1.5	0.05 ± 0.02	18

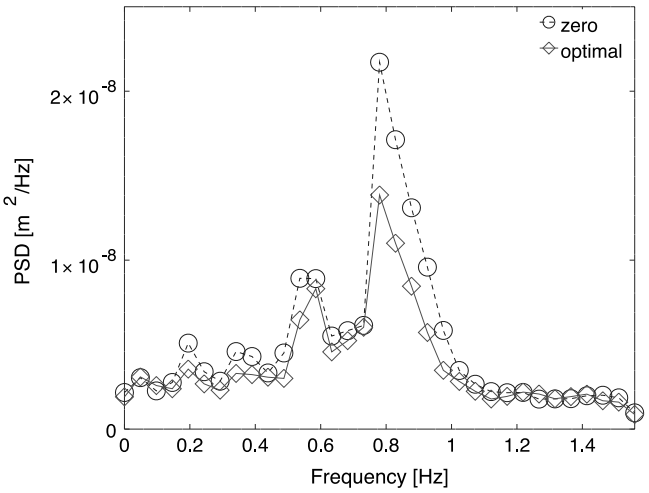

Fig. 19. Mean power spectral density measured by BPM MQD4BFF for both the zero gain case and the optimal gain case.

remove over 80% of this correlated component of the jitter. Some of the failure to perfectly remove the correlated component must undoubtedly be due to the limited resolution of the various components of the system (seismometer, BPM and kicker) but, for the result presented here, most of this effect is likely due to the generous range of gain settings that were considered optimal. By only considering those runs with a gain parameter of 125 the system could be quoted as having achieved a corrected jitter of 75.6 ± 1.6 μm. This represents a 17% reduction in the absolute beam jitter but, as this result is based on only three short data runs and the beam jitter is clearly fluctuating by a large amount, the nearby gain settings of 130 and 150 were considered equivalent in an attempt to produce an "on" data set with a similar amount of statistics to the zero-gain "off" data set.

Fig. 19 shows the effect of the feed-forward system on the power spectral density measured at the BPM. It can be seen that most peaks in the zero gain spectrum are reduced in the optimal gain case. The biggest reduction (35%–40%) is achieved in the 0.78 to 0.97 Hz region where the aliased versions of the 11.55 and 24.14 Hz peaks which dominate the quadrupole spectrum appear.

5. Conclusions and future work

Dynamic misalignment of the quadrupole magnets presents a real challenge to the maintenance of a beam of the required luminosity for a future linear collider. The novel technique of compensation of orbit distortion due to quadrupole motion using feed-forward control would be able to compensate for higher frequency oscillations than conventional beam orbit feedback, with lower cost and less of the integration issues than are associated with quadrupole stabilization systems.

The technique was demonstrated for the first time at the KEK ATF where it was able to eliminate 80% of the component of the final focus beam jitter that was due to the motion of the upstream quadrupole.

Future work will focus on introducing additional sensors and actuators to the feed-forward system. There are many additional seismometers that could be easily incorporated into the feed-forward system by making relatively trivial changes to the algorithm for calculating the correction. However, as described in Section 2.3.2, not all of them would be expected to make much difference. In terms of actuators a second identical stripline kicker exists just a few metres downstream of the first at a 90° betatron phase advance and, as the FONT5 board is designed to operate a pair of kickers simultaneously, it would be relatively straightforward to also include this second kicker as part of the existing system. Alternatively a third stripline kicker immediately upstream of the IP chamber could be used to compensate for vibrations of the final focus quadrupoles QF1FF and QD0FF, although this approach would likely require a separate FONT5 board located in the IP region.

Acknowledgements

We would like to thank our Japanese colleagues from the ATF international collaboration for the beam time required to gather the results presented here. In addition, we are grateful to the FONT team from the University of Oxford for the use of their hardware and for their support in integrating it into the feed-forward system. This research project was supported, in part, by the European Commission's Horizon 2020 Programme through the Marie S.-Curie RISE project E-Jade, Contract No. 645479.

References

[1] K. Kubo, Estimation of orbit change and emittance growth due to random misalignment in long linacs, Phys. Rev. ST Accel. Beams 14 (2011).
[2] J. Resta-López, P. Burrows, G. Christian, Luminosity performance studies of the Compact Linear Collider with intra-train feedback system at the interaction point, JINST 5 (2010).
[3] T. Himel, FEEDBACK: Theory and accelerator applications, Annu. Rev. Nucl. Part. Sci. 47 (1997).
[4] International Linear Collider Reference Design Report, Vol. 3, ILC Technical Report No. ILC-Report-2007-001 (2007).
[5] CLIC Conceptual Design Report, Vol. 3, CERN Technical Report No. CERN-2012-007 (2007).
[6] I. Reyzl, Stabilization of beam interaction in the TESLA linear collider, in: Proceedings of the 2000 European Particle Accelerator Conference, 2000.
[7] C. Montag, Active stabilization of mechanical quadrupole vibrations for linear colliders, Nucl. Instrum. Methods Phys. Res. A 378 (1996).
[8] C. Collette, S. Janssens, K. Artoos, A. Kuzmin, P. Fernandez-Carmona, M. Guinchard, R. Leuxe, C. Hauviller, Nano-motion control of heavy quadrupoles for future particle colliders: An experimental validation, Bull. Seismol. Soc. Amer. 102 (2012).
[9] G. Balik, B. Caron, J. Allibe, A. Badel, J.P. Baud, L. Brunetti, G. Deleglise, A. Jeremie, R.L. Breton, S. Vilalte, Sub-nanometer active seismic isolator control, J. Intell. Math. Syst. Struct. 24 (2013).
[10] A. Gaddi, H. Gerwig, N. Siegrist, F. Ramos, Dynamic analysis of the final focusing magnets pre-isolator and support system, LCD-Note-2010-11 (2010).
[11] J. Pfingstner, K. Artoos, C. Charrondière, S. Janssens, M. Patecki, Y. Renier, D. Schulte, R. Tomás, A. Jeremie, K. Kubo, S. Kuroda, T. Naito, T. Okugi, T. Tauchi, N. Terunuma, Mitigation of ground motion effects in linear accelerators via feed-forward control, Phys. Rev. ST Accel. Beams 17 (2014).
[12] F. Hinode, S. Kawabata, H. Matsumoto, K. Oide, K. Takata, S. Takeda, J. Urawaka, Accelerator Test Facility: Design and study report, KEK Technical Report No. 95-4 (1995).
[13] https://www.guralp.com/documents/DAS-T60-0001.pdf.
[14] Y. Renier, J. Pfingstner, R. Tomás, D. Schulte, Detection of ground motion effects on the beam trajectory at ATF2, in: Proceedings of the 2012 International Particle Accelerator Conference, 2012.
[15] Y.I. Kim, R. Ainsworth, A. Aryshev, S.T. Boogert, G. Boorman, J. Frisch, A. Heo, Y. Honda, W.H. Hwang, J.Y. Huang, E.-S. Kim, S.H. Kim, A. Lyapin, T. Naito, J. May, D. McCormick, R.E. Mellor, S. Molloy, J. Nelson, S.J. Park, Y.J. Park, M. Ross, S. Shin, C. Swinson, T. Smith, N. Terunuma, T. Tauchi, J. Urakawa, G.R. White, Cavity beam position monitor system for the Accelerator Test Facility 2, Phys. Rev. ST Accel. Beams 15 (2012).
[16] http://www.aps.anl.gov/epics/.
[17] https://confluence.slac.stanford.edu/display/ATF/ATF2+Flight+Simulator.
[18] J.W. Eaton, D. Bateman, S. Hauberg, R. Wehbring, GNU Octave version 4.2.0 manual: a high-level interactive language for numerical computations, 2016. URL http://www.gnu.org/software/octave/doc/interpreter.
[19] B. Bolzon, Etudes des Vibrations et de la Stabilisation à L'échelle Sous-Nanométrique des Doublets Finaux D'un Collisionneur Linéaire (Ph.D. thesis), Université de Savoie, 2007.
[20] J. Proakis, D. Manolakis, Digital Signal Process, Macmillan Publishing Company, New York, 1992.
[21] D.R. Bett, C. Charrondière, M. Patecki, J. Pfingstner, D. Schulte, R. Tomás, A. Jeremie, K. Kubo, S. Kuroda, T. Naito, T. Okugi, T. Tauchi, N. Terunuma, Improving the performance of an orbit feed-forward based on quadrupole motion at the KEK ATF, in: Proceedings of the 2017 International Particle Accelerator Conference, 2017.
[22] P.D. Welch, The use of fast Fourier transforms for the estimation of power spectra: A method based on time averaging over short modified periodograms, IEEE Trans. Audio Electroacoust. 15 (1967).
[23] D.R. Bett, The development of a fast intra-train beam-based feedback system capable of operating on the bunch trains of the International Linear Collider (D.Phil. thesis), University of Oxford Physics Department, 2013.
[24] http://www-pnp.physics.ox.ac.uk/font/index.html.
[25] B.D. Constance, Design and Beam Testing of a Fast, Digital Intra-train Feedback System and its Potential for Applications at the International Linear Colider (D.Phil. thesis), University of Oxford Physics Department, 2011.